AGU PUBLICATIONS

Geophysical Research Letters

RESEARCH LETTER
10.1002/2016GL071932

Key Points:
- Water vaporization was "observed" in high-velocity friction experiments
- Water vaporization promotes fluid pressurization during coseismic slip
- Water vaporization limits the temperature rise during coseismic slip

Supporting Information:
- Supporting Information S1

Correspondence to:
J. Chen,
j.chen3@uu.nl

Citation:
Chen, J., A. Niemeijer, L. Yao, and S. Ma (2017), Water vaporization promotes coseismic fluid pressurization and buffers temperature rise, *Geophys. Res. Lett.*, *44*, 2177–2185, doi:10.1002/2016GL071932.

Received 18 MAY 2016
Accepted 18 JAN 2017
Accepted article online 20 JAN 2017
Published online 6 MAR 2017

Water vaporization promotes coseismic fluid pressurization and buffers temperature rise

Jianye Chen[1,2], André Niemeijer[2], Lu Yao[1], and Shengli Ma[1]

[1]State Key Laboratory of Earthquake Dynamics, Institute of Geology, China Earthquake Administration, Beijing, China, [2]HPT Laboratory, Department of Earth Sciences, Utrecht University, Utrecht, Netherlands

Abstract We investigated the frictional properties of carbonate-rich gouge layers at a slip rate of 1.3 m/s, under dry and water-saturated conditions, while monitoring temperature at different locations on one of the gouge-host rock interfaces. All experiments showed a peak frictional strength of 0.4–0.7, followed by strong slip weakening to steady state values of 0.1–0.3. Experiments which used a pore fluid with a constant drainage path to the atmosphere showed the development of a temperature plateau beyond 100°C, contemporaneous with the dynamic slip weakening and consistent with thermodynamic considerations of ongoing vaporization of pore water. Upon pore fluid vaporization, the pore pressure increases, while the temperature is buffered endothermically, such that the pore water moves along the liquid-vapor transition curve in a pressure-temperature phase diagram. Pore fluid phase transitions of this kind are expected to occur in natural earthquakes at relatively shallow crustal levels, enhancing fluid pressurization while impeding the achievement of high temperatures. Therefore, the operation of vaporization may help explain the low downhole temperature anomalies obtained shortly after large earthquakes.

1. Introduction

Numerous high-velocity (HV) friction experiments have been performed in the last two decades, but the majority were at room humidity conditions [*Di Toro et al.*, 2011; *Niemeijer et al.*, 2012]. However, under natural in situ earthquake conditions, faults are expected to be subjected to water-saturated conditions, especially for the shallow portions where the principal slip zone materials usually consist of porous gouge material. Technical challenges related to pore fluid confinement have severely hindered the investigation of the role of water in HV frictional weakening [*Kitajima et al.*, 2011]. The wet experiments that have been done on bare rocks indicate that the presence of water could either promote or inhibit the dynamic weakening process, depending on the host-rock composition [*Violay et al.*, 2013, 2015], while for water-saturated gouges, derived from fault rocks or landslides, thermal pressurization of pore water was generally inferred to be the dominant mechanism controlling dynamic slip weakening [e.g., *Faulkner et al.*, 2011; *Ferri et al.*, 2011; *Ujiie et al.*, 2013; *Togo et al.*, 2014], although the state of the pore water (liquid or gaseous) and its role in causing the weakening is poorly understood [*Mizoguchi et al.*, 2007a; *Boutareaud et al.*, 2010; *Kitajima et al.*, 2010; *Ferri et al.*, 2010]. In some HV friction experiments, strong axial dilatation and intermittent bursts of water vapor out of the rotating sample assembly, past the confining Teflon sleeve, have been observed [e.g., *Kitajima et al.*, 2011; *Chen et al.*, 2013]. Numerical modeling of natural earthquakes shows that the local pressure-temperature conditions inside the slip zone can vary through a large range during faulting [e.g., *Wibberley and Shimamoto*, 2005], and the pore water may undergo multiple phase changes, from the liquid to supercritical states or to the vapor gaseous form [*Sulem et al.*, 2007; *Tanikawa and Shimamoto*, 2009]. Water vaporization is thus expected to be important since it may affect the propagation of seismic slip and the energy budget associated with an earthquake [*Noda and Lapusta*, 2013; *Kitajima et al.*, 2011], especially for the shallow depths of a fault. At these depths, downhole temperatures have been measured directly after large earthquakes, which were subsequently used to infer the apparent dynamic friction of the slipping zone of the fault during the earthquakes [e.g., *Li et al.*, 2015].

In this work, we examine whether water vaporization occurs in a water-saturated gouge layer during seismic slip and whether it affects the slip-weakening process. By making a small change to the sample assembly typically used in HV friction experiments, we are able to simulate a constant fluid drainage boundary condition for the sample as well as measure the temperature evolution on one of the gouge-host rock

interfaces as a function of radial position. Our results indicate that under specific conditions, vaporization of pore water can occur, causing a significant delay in the temperature rise while enhancing fluid pressurization and thus dynamic weakening compared to standard "undrained" or dry experiments.

2. Material and Methods

Friction experiments were performed on gouge material obtained by crushing a carbonate fault breccia, collected from the Yingxiu-Beichuan Fault which hosted the 2008 Wenchuan earthquake, Sichuan, China [*Xu et al*., 2009; *Chen et al*., 2013]. Powdered material of the sample, consisting of calcite (68%), dolomite (29%), minor quartz (1%), and clay (1%, smectite-illite mixed layer), was sieved to obtain a grain-size fraction of $<125\,\mu$m to form the starting material.

Friction experiments were performed at a slip rate of 1.3 m/s and varied normal stresses (σ_n) from 0.4 to 2.2 MPa, using the HV frictional apparatus installed in Beijing (see details in *Ma et al*. [2014]). Using slightly different sample assemblies, we simulated "room humidity," "wet, boundaries less permeable," and "wet, boundaries permeable" conditions (hereafter referred to as "dry," "wet I," and "wet II" experiments, respectively). For the dry and wet I experiments, a conventional sample assembly was employed, which includes a gouge layer and a pair of rock cylinders surrounded by a tightly fitting Teflon sleeve (Figure 1a). For the wet II experiments, a four-layered sieving mesh was placed between the lower (stationary) cylinder and the Teflon sleeve (Figure 1b), which prevents gouge leakage but allows for the pore fluid to be drained to the atmosphere with a constant fluid conductivity. Other components are as in the conventional one. The wall rock (Indian gabbro) used is 40 mm in diameter with rough end surfaces (ground with #80 SiC powder) and practically impermeable (~10^{-22} m^2). In each experiment, 2.3 g of the gouge was placed between the two gabbro cylinders. For the wet I ones, to fulfill the water-saturated condition, we added ~0.4 mL of deionized H_2O as calculated from the gouge thickness, while for the wet II ones, more than 1 mL water was added since the excess water could escape from the mesh upon applying a normal stress. An axial force corresponding to the normal stress applied was then imposed and maintained constant for 5 min, producing a layer thickness of ~1.2 and 1.0 mm for the dry and wet gouges, respectively. The gouge was then pretreated by sliding at a slow slip rate (1.3 mm/s) for ~60 s to suppress the pressurization effects due to gouge compaction, at which point the slip rate was increased quasi-instantaneously to 1.3 m/s (within 0.2 s), which lasted for 20–25 s.

Besides the three sets of experiments addressed above, we conducted a repeat experiment and two control experiments, all at 1 MPa and wet II condition. One control experiment was run without preslip, and for the other, a porous ceramic, with a porosity of 29.3% and a composition similar to andalusite, was used as the upper cylinder, of which the permeability is determined to be 3.0×10^{-14} m^2 at 2 MPa. All the experiments involved are listed in Table S1 in the supporting information. Data reduction followed *Ma et al*. [2014]. Apparent friction coefficient (μ) was determined as the ratio of the shear stress measured to the applied normal stress, thereby ignoring cohesion. The shear resistance exerted by Teflon sleeve was corrected according to the experiments performed on empty samples.

To measure temperatures on the sliding surface during shear, manually welded Ni-Cr thermocouple wires, insulated by corundum tubes, were embedded into the lower (stationary) cylinder that had been drilled beforehand at radial distances of 0, 7 and 14 mm from the center (Figure 1b). We glued the thermocouples with high-temperature cement near the surface of the cylinder and with epoxy at the remote end, setting the welding points ($<$0.5 mm in diameter) exactly on the grinding end surface of the cylinder. An additional thermocouple was pierced through the Teflon sleeve to measure the temperature at the edge of the gouge layer.

3. Results

The friction data from the three sets of experiments are summarized in Figures 1c–1h (see also Table S1). Specifically, the dry tests displayed frictional behavior that has been recognized in previous studies [e.g., *Smith et al*., 2013; *Di Toro et al*., 2011; *Rempe et al*., 2014]. The peak friction coefficients, μ_{pk}, are ~0.7, and the postpeak slip-weakening curves show a positive correlation with the applied normal stress (σ_n), i.e., the higher σ_n, the quicker slip weakening occurs (Figure 1c). The steady state friction coefficients μ_{ss} and

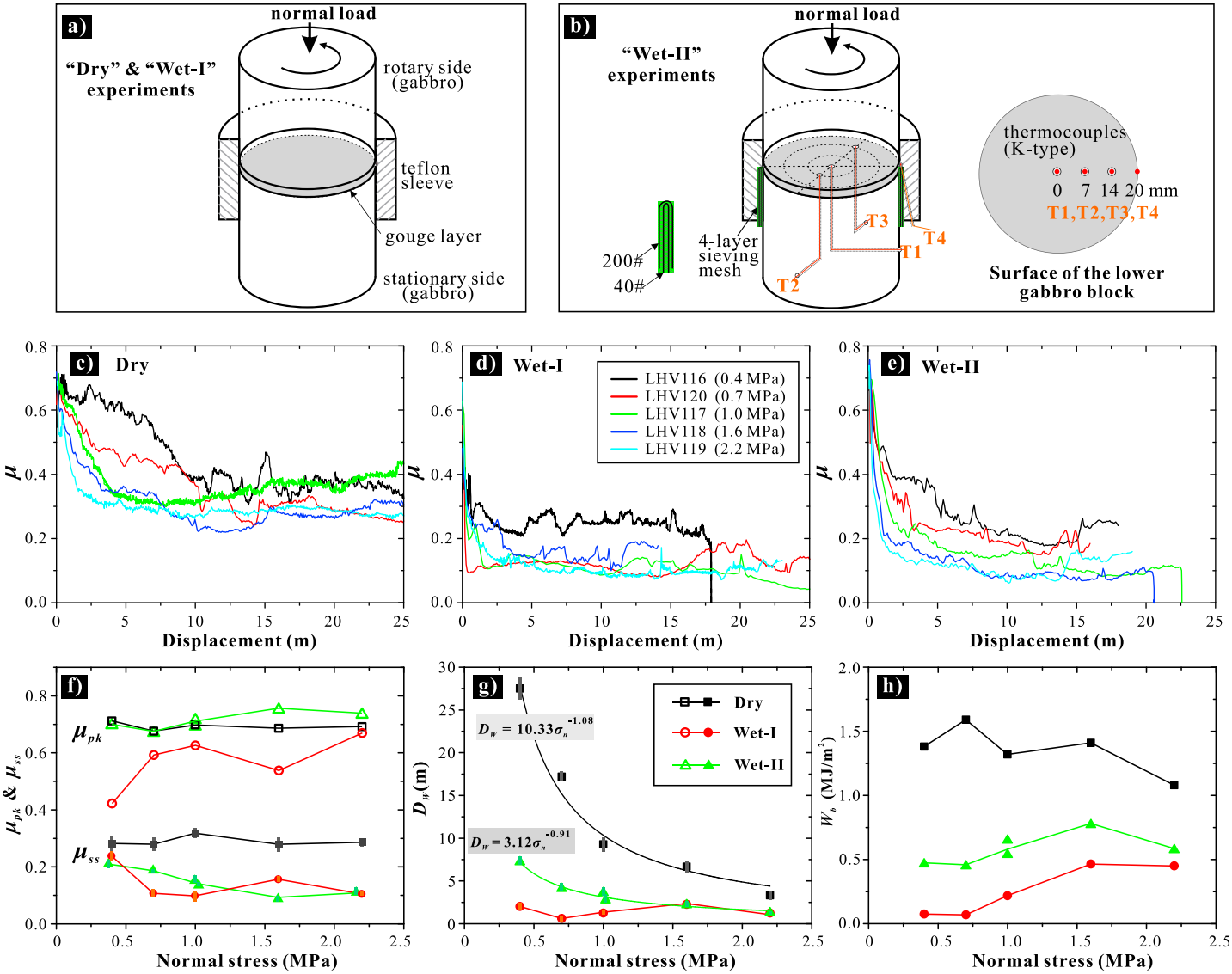

Figure 1. Sample assemblies used for rotary-shear high-velocity experiments under (a) dry and wet I and (b) wet II conditions. In case Figure 1b, thermocouples were set on the gouge-wall rock interface to measure temperature. See details of the sample assemblies and thermocouple settings in the text. (c–e) Evolution of apparent friction coefficient (μ = shear stress/normal stress, ignoring cohesion) with shear displacement, for the three sets of experiments, respectively. Each plot shows five tests performed at different normal stresses (0.4–2.2 MPa). (f–h) The presentation of the frictional parameters derived from these experiments as a function of applied normal stress, i.e., (f) peak and steady state friction coefficients, μ_{pk}, and μ_{ss}, (g) slip-weakening distance D_w, and (h) breakdown work W_b. The μ_{pk} values were directly picked from the friction curves, and the μ_{ss} and D_w values were determined by fitting the postpeak friction curves with an exponential equation given by *Mizoguchi et al.* [2007a, 2007b], with the error bars representing a 95% confidence level for the fitting. Note that for wet II data, results from a repeat test (LHV369) are added.

slip-weakening distances D_w were determined by fitting the postpeak friction curves with Mizoguchi's equation [*Mizoguchi et al.*, 2007b]. The μ_{pk} and μ_{ss} values obtained from the dry experiments are not sensitive to σ_n (Figure 1f), while D_w values decrease according to a power law for increasing σ_n (Figure 1g). In the wet I experiments, where the pore fluid resided within the gouge porosity, enclosed by the two gabbro cylinders and the Teflon sleeve, the frictional behavior was characterized by low peak stress and by rapid attainment of steady state (Figure 1d). The μ_{pk} and μ_{ss} values were lower than the dry results but varied in an unpredictable manner with σ_n (Figure 1f). Moreover, no systematic relation between σ_n and D_w was evident (Figure 1g). In the wet II experiments, the pattern of friction coefficient versus displacement was similar to the dry results and showed systematic changes with σ_n (Figure 1c). The μ_{pk}

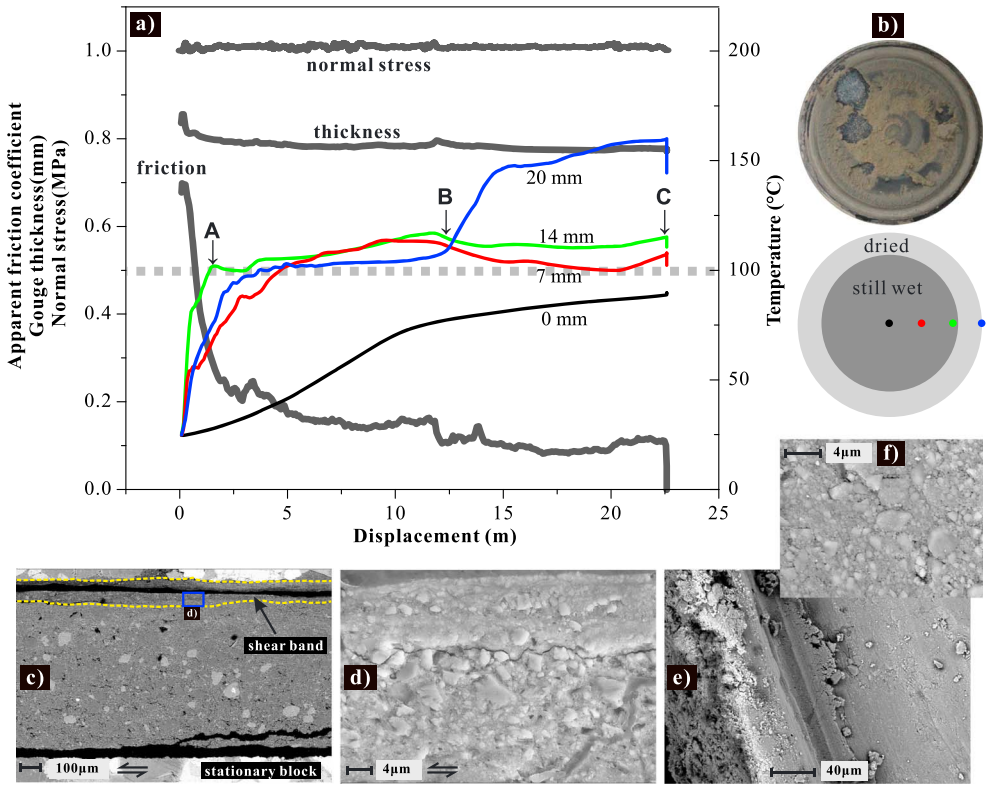

Figure 2. (a) Evolution of apparent friction coefficient, normal stress, and gouge thickness, as well as temperatures at different radial positions on the gouge layer, with shear displacement, for a representative wet II experiment (LHV366). The absolute thickness of a gouge layer was calculated using the axial position measured during shear relative to the axial position of the empty sample which was determined before the experiment. Note that the axial displacement data were not corrected for any thermal expansion of the sample assembly and apparatus. The temperature results indicate an existence of a near-constant temperature plateau at ~100°C (A→C). More results about the temperature plateau are shown in the supporting information. (b) Photograph and interpretative sketch of the splitted sample showing the dried condition of the gouge layer after the experiment (LHV369). (c–f) Scanning electron microscopy images of postexperimental samples. Figures 2c and 2d are from a thin section made of LHV366, and Figures 2e and 2f are from the slip surfaces recovered from LHV372. Figures 2c, 2e, and 2f are backscattered electron images, and Figure 2d is a secondary electron image.

values were uniform, while the μ_{ss} values showed a decrease with increasing σ_n. The D_w values showed a power law decay with σ_n but were smaller than those obtained in the dry tests (Figure 1g). Finally, the breakdown work, W_b, as calculated from the μ_{pk}, μ_{ss}, and D_w values determined following *Togo et al.* [2011], displayed a decreasing trend from the dry (1.08–1.87 MJ/m^2), via the wet II (0.449–0.771 MJ/m^2) to the wet I experiments (0.05–0.515 MJ/m^2).

Figure 2a compares the evolution of apparent friction coefficient, normal stress, and gouge thickness, as well as temperatures at different radial positions on the gouge layer, for a typical wet II experiment (LHV366). The normal stress was well controlled (with <2% fluctuations), and the gouge layer compacted ~0.05 mm upon initiation of the HV sliding (<0.35 m) and then maintained a near-constant thickness throughout the experiment. The temperatures at the three outer temperature measurement points (TMPs) rose rapidly at <1.6 m displacement (as annotated by arrow "A") and then turned almost flat at ~100°C and remained at this temperature for the remainder of slip (A→"C"), with the exception of the temperature at the 20 mm TMP. The temperature here increased abruptly from ~100°C after about 12 m slip, reaching a maximum of 153°C by the end of slip ("B"→C). Correspondingly, temperatures at 7 mm and 14 mm TMPs showed slight decreases. The temperature measured at the central point was below 100°C throughout the experiment. After splitting the sample assembly immediately after the experiment, we found that 6 mm of the outer radius of the gouge layer had turned dry (color changed from dark grey to light grey, Figure 2b). Microstructural analysis revealed that the shear was mostly

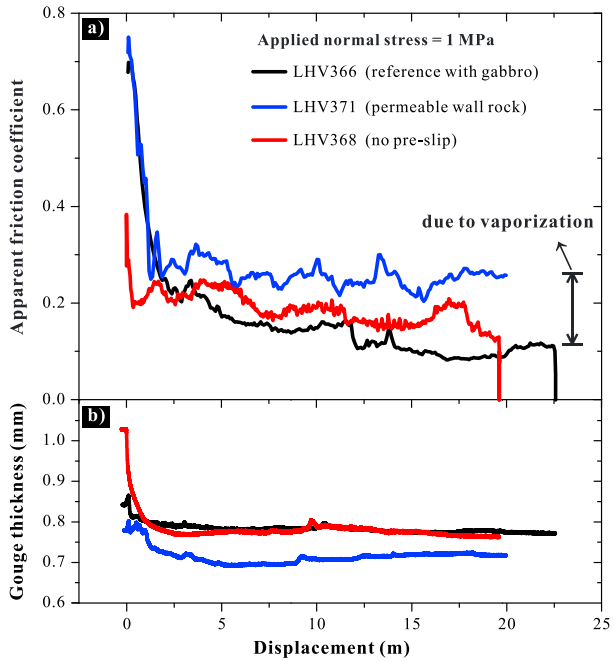

Figure 3. Results of two control experiments with no preslip and permeable wall rock, showing the evolution of (a) apparent friction coefficient and (b) gouge thickness with shear displacement. The results from the reference case (LHV366) are added for comparison.

localized to boundary shear bands developed close to the rotary host rock, along which the gouge layer split during sample recovery (Figure 2c). The shear bands, of 50–100 μm thickness, were characterized by pronounced grain size reduction (Figure 2d), with most particles in the bands being <4 μm in diameter, and angular, exhibiting a chaotic, granular microstructure (Figures 2e and 2f).

The repeat experiment performed at the same condition showed consistent mechanical data and almost reproducible temperature evolution results, including the flat temperature profiles or plateaus at ~100°C, as well as the subsequent deviation at the 20 mm TMP (Figure S1). Similar temperate plateaus were observed in other wet II experiments at varied normal stresses, except the one performed at 2.2 MPa, in which almost the entire gouge layer became dry after the experiment (Figure S2). By contrast, this temperature plateau was not visible in the dry test performed under otherwise the same conditions, in which the temperatures at all the four TMPs showed a more or less continuous rise with the passage of slip (Figure S3). In the control experiment without preslip, the evolution of apparent friction coefficient displayed a very low peak value (0.38) and a sharp reduction in the very first centimeters of the slip, reaching a steady state (0.22) at ~0.2 m displacement (Figure 3a). Compared with the reference test (LHV366), this experiment showed a remarkable reduction in gouge layer thickness upon initiation of the HV sliding (Figure 3b). Again, a near-constant temperature of 100°C was observed at the edge of the gouge layer, but at the 14 mm TMP it just rose continuously (Figure S4a). The control test with porous wall rock displayed similar results to the reference test, except that it showed higher steady state friction coefficient at >2 m displacement, which is at about the dry level (Figure 3a and Table S1). This experiment also showed relatively high temperature rises, but still a temperature plateau at and above 100°C can be discerned for most of the duration of sliding (Figure S4b).

4. Interpretation and Discussion

Our dry samples show slip-weakening behavior and microstructures similar to previous studies on carbonate material (Figures 1 and S3), and similar slip-weakening mechanisms (i.e., flash heating, decomposition, intracrystalline plasticity, and/or grain boundary sliding) might be inferred to be involved [e.g., *Smith et al.*, 2013, 2015; *De Paola et al.*, 2015]. The wet samples, at both wet I and wet II conditions, show lower μ_{ss} and smaller D_w and W_b values than the dry results (Figure 1). As many previous studies, this can be generally explained by pore fluid pressurization [*Ferri et al.*, 2010; *Ujiie et al.*, 2011; *Faulkner et al.*, 2011; *Bullock et al.*, 2015]. Specifically, in the wet I experiments, the gouge layer was subjected to an uncertain fluid-flow boundary condition due to the poor and variable sealing capacity of the Teflon sleeves, such that the pressurized fluid, probably produced by thermal pressurization [e.g., *Faulkner et al.*, 2011], can bleed off in an unpredictable manner during the experiments. This results in an absence of systematic relationships between the friction parameters (μ_{pk}, μ_{ss}, and D_w) and normal stress and causes difficulties in interpreting and underpinning the mechanisms operating in the experiments as well as with potential extrapolations of the experimental results to natural conditions. The following discussion will focus on the wet II results, from which two observations are of particular interest.

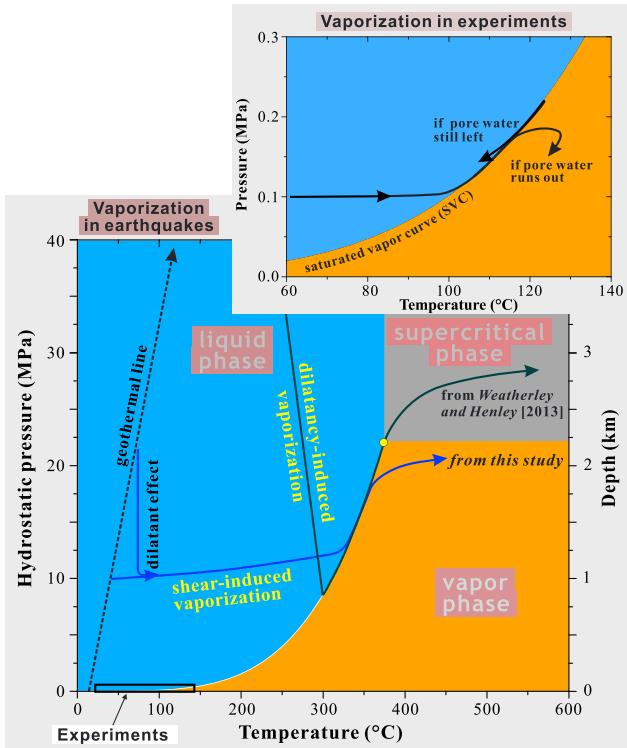

Figure 4. Evolution of the PT state of pore fluid interpreted from the experiments and the extrapolation to natural earthquake conditions. The scenario of dilatancy-induced vaporization proposed by *Weatherley and Henley* [2013] is added.

4.1. The Key Observations

First, with a fixed drainage boundary condition of pore fluid pressure for the gouge layer, systematic friction data were obtained (i.e., μ versus displacement and μ_p, μ_{ss}, and D_w versus normal stress, Figure 1). In particular, the peak friction coefficients are all at ~0.7, similar to the dry results, while the steady state values are lower than the dry results and show a decreasing trend with increasing normal stress. Higher normal stress implies that more frictional heating can be generated, while the gouge layer is expected to be less permeable [*Tanikawa et al.*, 2015]. In general, this will result in more efficient fluid pressurization, giving rise to a lower effective normal stress and therefore faster slip-weakening (smaller D_w) and lower apparent dynamic friction (smaller μ_{ss}). A similar reasoning applies to the control experiment with permeable wall rock, in which higher μ_{ss} was observed (Figure 3) [see also *Faulkner et al.*, 2011; *Ujiie et al.*, 2013].

Second, our temperature measurements revealed the widespread occurrence of plateaus in the temperature evolution curves, along which the temperatures remain constant or increase slightly at and above 100°C. We infer that this near-constant temperature corresponds to the vaporization of pore water, and the slight increases (e.g., A→B in Figure 2a) imply that the pore fluid is moving along the saturated vapor curve (SVC, also referred to as liquid-vapor transition curve) in the pressure-temperature (PT) phase diagram (Figure 4). Once the temperature reaches the boiling temperature, pore water begins to vaporize and pore pressure will increase due to a volume expansion of ~1700 times (0.001→1.680 m^3/kg at 100°C). Besides the direct effect of a lower effective normal stress on frictional heating, this will further inhibit temperature rise due to the enthalpy change associated with the phase change. As long as liquid water is present, i.e., the gouge is not drying, the local PT-state is expected to evolve along the SVC, and temperature should remain constant at ~100°C if excess pore pressure is able to drain fast enough. This is confirmed by our observation that the TMPs, at which the temperature curves showed a deviation from the 100°C plateau (abrupt rise), always coincide with the dried area after the experiments (Figures 2, S1, and S2).

4.2. Slip-Weakening Mechanisms

The control experiment with porous ceramic (LHV371) showed an almost identical slip-weakening curve as the reference case for the first 2 m displacement (Figure 3a), indicating that any fluid pressurization was not efficient before the onset of vaporization. We attributed this to the permeable boundary conditions of these experiments: any fluid pressurization by pure thermal expansion of pore water (thermal pressurization) would be rapidly dissipated via fluid flow. This interpretation is consistent with the constant gouge layer thickness observed (Figure 2a) and was confirmed by an additional test in which pressure transducers instead of thermocouples were placed into the lower host-rock cylinder (see the supporting information). In this test, negligibly small pore pressure rises were observed at displacements less than ~2 m. By virtue of the low temperatures measured and the lack of typical macro/microstructures (e.g., mirror-like surfaces and decarbonation vesicles, Figures 2c–2f), we infer that the slip-weakening mechanisms possibly operating in

the dry experiments (i.e., decarbonation, dynamic recrystallization, and superplasticity) are unlikely to be dominant mechanism(s). From the recent study by *Yao et al*. [2016] and the absence of widespread nanoparticles, nanopowder lubrication is an improbable mechanism as well (Figure 2f). Based on the above considerations, we propose that flash heating of asperities is the most likely mechanism responsible for the incipient slip weakening observed in the wet II experiments (although its effect could also be suppressed by the buffered macrotemperature) [e.g., *Rice*, 2006; *Platt et al*., 2014], and with successive slip, pore water vaporization begins to contribute to the weakening.

An obvious next question is how much weakening was attributed to vaporization? In our test with permeable ceramics (LHV371), high pressure cannot be sustained due to the quick drainage to atmosphere, then all the weakening observed should be caused by thermally activated mechanisms such as flash heating. Based on similar temperature evolution, we argue that these mechanisms also operated in the reference test (LHV366) and contributed similarly to the weakening observed. This means that any difference observed in the final steady states of these two experiments must be related to fluid pressurization. Since thermal pressurization was not possible as temperatures hardly increased, then vaporization was responsible. As indicated in Figure 3a, a comparison of the two friction curves indicates that vaporization can cause a drop in the apparent friction coefficient by at least 0.1. Alternatively, since our thermocouples reflect temperatures on one of the gouge-host rock interfaces, we can estimate the minimum pore pressure based on the phase diagram. The rationale for doing this is also supported by the fact that the temperature plateaus shown by the 20 mm TMPs are always close to 100°C since it is open to atmosphere (e.g., Figure 2), while the plateaus shown by the inner TMPs can be higher than 100°C, implying excess pore pressure and indicating that the fluid at these positions follow the SVC. For instance, a maximum temperature of 116°C was measured by the 14 mm TMP in LHV366 which would indicate a local pore pressure of at least 0.15 MPa (Figure 4) or an absolute reduction in local apparent friction coefficient of 0.05. Considering the existence of thermal gradients in the gouge layer, especially the fact that slip was localized on the opposite side away from the thermocouples (i.e., at ~1 mm distance), the pore pressures within the shear band, relying on the local temperatures with relation to the SVC, could be much higher. This interpretation was further confirmed by the additional experiment, in which the average pore pressure rise measured reached ~0.35 MPa, corresponding to an apparent frictional weakening of ~0.25 (see the supporting information).

The control test without preslip implies a potential role of shear-induced compaction in influencing the dynamic weakening (Figure 3a). The pore water, extruded from the gouge due to compaction, can generate an immediate rise in pore pressure, allowing low friction to be attained in the early stage of slip [e.g., *Ferri et al*., 2011]. However, this is probably not the case for natural earthquakes, especially for those on mature faults where the gouges have been subjected to interseismic compaction and cementation [*Marone et al*., 1990; *Hickman et al*., 1995]. On the contrary, considering the irregularities of natural fault surfaces and the increasing strain rate in a dynamic loading process, shear-induced dilatancy is the more likely natural situation [*Rice*, 2006; *Marone et al*., 1990], although we cannot exclude compaction-induced weakening when ruptures branch into adjacent high-porosity breccia zones [e.g., *Boutareaud et al*., 2008].

4.3. Implications to Nature

The kinetics of water vaporization is fast [*Mizoguchi et al*., 2007a], and it starts at relatively low temperatures at lower pressures (Figure 4). Even though our results were obtained for carbonate, vaporization should operate in any type of fault gouge. Water vaporization is therefore expected to be readily involved in natural earthquakes, at least in large ones (e.g., the 1999 Chi-Chi earthquake and the 2008 Wenchuan earthquake), during which the coseismic ruptures have propagated to the surface. As shown by our experiments, water vaporization has a significant endothermic effect [see also *Kitajima et al*., 2011; *Brantut et al*., 2011]. Meanwhile, vaporization should also have a great potential for generating high pore pressure, as discussed above, thereby lowering the apparent frictional strength [*Sulem et al*., 2007]. Assuming that vaporization did occur, both effects may help explain the lack of temperature anomalies measured for the principal shear zones of the above mentioned earthquakes at 0.3–0.6 km depths in the drilling campaigns executed shortly after the earthquakes [e.g., *Kano et al*., 2006; *Tanaka et al*., 2006; *Li et al*., 2015]. According to the phase diagram (Figure 4), at these depths, water vaporization can occur as long as the local temperature reaches the critical value of 234–276°C. If this is the case, the dynamic friction coefficient inferred from the temperature-logging data of the drillings will be underestimated. Note that the phase transition of water is a reversible process so

that the frictional heat stored in the heated vapor phase will be released by condensation in the postseismic period, but likely over a large space and time. Finally, we infer that this phase transition may also occur at greater depths. If shear-induced dilatancy occurs, it can cause a pore suction within the fault zone, leading to a quasi-instantaneous drop in pore pressure. As evidenced by the presence of high-grade gold deposits in fault zones, the earthquake-induced dilatant process can even directly result in flash vaporization [*Sibson et al*., 1988; *Weatherley and Henley*, 2013; *Peterson and Mavrogenes*, 2014; *Cox and Munroe*, 2016] (Figure 4).

Our present work to date indicates the possibility of water vaporization during seismic slip. However, to gain a clear idea of the condition(s) for its occurrence in natural earthquakes and to evaluate the resultant temperature buffering, fluid pressurization and fault weakening effects, experimental work is of limited use, because the process depends very much on the experimental configuration (e.g., normal stress, gouge permeability, boundary conditions, and dimensions of the sample assembly). Recent modeling studies are now leading to an improved understanding of coseismic thermal pressurization and reaction processes and of their influence on fault rupture propagation [e.g., *Brantut et al*., 2010; *Noda and Lapusta*, 2013]. Beyond the scope of experimental studies, it is important for these models to include the phase transition of the fluid, which also necessitates a description of the evolution of permeability of the slipping zone and its surroundings as well as shear-induced dilatation. It is also critical to include water vaporization when simulating HV friction experiments; otherwise, the temperature rise can easily be overestimated [e.g., *Ujiie et al*., 2013]. Finally, it should be stressed that the temperatures measured in this study only reflected the macrotemperatures of the gouge layer. The local flash temperatures at the active asperities could be higher due to flash heating or local drying of the gouge.

Acknowledgments
Jianye Chen is funded by the European Research Council starting grant SEISMIC (335915), the State Key Laboratory of Earthquake Dynamics (LED2014A06), and the national Natural Science Foundation of China (41404143). André Niemeijer is funded by SEISMIC (335915) and the Netherlands Organisation for Scientific research (NWO) VIDI grant (nr. 854.12.011). We thank the reviewers for their constructive review comments.

References

Boutareaud, S., C. A. J. Wibberley, O. Fabbri, and T. Shimamoto (2008), Permeability structure and co-seismic thermal pressurization on fault branches: Insights from the Usukidani Fault, Japan, in *The Internal Structure of Fault Zones: Mechanical and Fluid Flow Properties*, *Spec. Publ. Geol. Soc*., vol. 299, edited by C. A. J. Wibberley et al., pp. 341–361.

Boutareaud, S., A.-M. Boullier, M. Andréani, D.-G. Calugaru, P. Beck, S.-R. Song, and T. Shimamoto (2010), Clay-clast aggregates: New textural evidence for seismic faulting, *J. Geophys. Res.*, *115*, B02408, doi:10.1029/2008JB006254.

Brantut, N., A. Schubnel, J. Corvisier, and J. Sarout (2010), Thermochemical pressurization of faults during coseismic slip, *J. Geophys. Res.*, *115*, B05314, doi:10.1029/2009JB006533.

Brantut, N., R. Han, T. Shimamoto, N. Findling, and A. Schubnel (2011), Fast slip with inhibited temperature rise due to mineral dehydration: Evidence from experiments on gypsum, *Geology*, *39*, 59–62.

Bullock, R. J., N. De Paola, and R. E. Holdsworth (2015), An experimental investigation into the role of phyllosilicate content on earthquake propagation during seismic slip in carbonate faults, *J. Geophys. Res. Solid Earth*, *120*, 3187–3207, doi:10.1002/2015JB011914.

Chen, J., X. Yang, Q. Duan, T. Shimamoto, and C. J. Spiers (2013), Importance of thermochemical pressurization in the dynamic weakening of the Longmenshan Fault during the 2008 Wenchuan earthquake: Inferences from experiments and modeling, *J. Geophys. Res. Solid Earth*, *118*, 4145–4169, doi:10.1002/jgrb.50260.

Cox, S. F., and S. M. Munroe (2016), Breccia formation by particle fluidization in fault zones: Implications for transitory, rupture-controlled fluid flow regimes in hydrothermal systems, *Am. J. Sci.*, *316*, 241–278.

De Paola, N., R. E. Holdsworth, C. Viti, C. Collettini, and R. Bullock (2015), Can grain size sensitive flow lubricate faults during the initial stages of earthquake propagation?, *Earth Planet. Sci. Lett.*, *43*, 48–58.

Di Toro, G., R. Han, T. Hirose, N. De Paola, S. Nielsen, K. Mizoguchi, F. Ferri, M. Cocco, and T. Shimamoto (2011), Fault lubrication during earthquakes, *Nature*, *471*, 493–499.

Faulkner, D. R., T. M. Mitchell, J. Behnsen, T. Hirose, and T. Shimamoto (2011), Stuck in the mud? Earthquake nucleation and propagation through accretionary forearcs, *Geophys. Res. Lett.*, *38*, L18303, doi:10.1029/2011GL048552.

Ferri, F., G. Di Toro, T. Hirose, and T. Shimamoto (2010), Evidence of thermal pressurization in high-velocity friction experiments on smectite rich gouges, *Terra Nova*, *22*, 347–353.

Ferri, F., G. Di Toro, T. Hirose, R. Han, H. Noda, T. Shimamoto, M. Quaresimin, and N. de Rossi (2011), Low- to high-velocity frictional properties of the clay-rich gouges from the slipping zone of the 1963 Vaiont slide, northern Italy, *J. Geophys. Res.*, *116*, B09208, doi:10.1029/2011JB008338.

Hickman, S., R. Sibson, and R. Bruhn (1995), Introduction to special section: Mechanical involvement of fluids in faulting, *J. Geophys. Res.*, *100*(B7), 12,831–12,840, doi:10.1029/95JB01121.

Kano, Y., J. Mori, R. Fujio, H. Ito, T. Yanagidani, S. Nakao, and K.-F. Ma (2006), Heat signature on the Chelungpu fault associated with the 1999 Chi-Chi, Taiwan earthquake, *Geophys. Res. Lett.*, *33*, L14306, doi:10.1029/2006GL026733.

Kitajima, H., J. S. Chester, F. M. Chester, and T. Shimamoto (2010), High speed friction of disaggregated ultracataclasite in rotary shear: Characterization of frictional heating, mechanical behavior, and microstructure evolution, *J. Geophys. Res.*, *115*, B08408, doi:10.1029/2009JB007038.

Kitajima, H., F. M. Chester, and J. S. Chester (2011), Dynamic weakening of gouge layers in high-speed shear experiments: Assessment of temperature-dependent friction, thermal pressurization, and flash heating, *J. Geophys. Res.*, *116*, B08309, doi:10.1029/2010JB007879.

Li, H., et al. (2015), Long-term temperature records following the M_w 7.9 Wenchuan (China) earthquake consistent with low friction, *Geology*, *43*(2), 163–166.

Ma, S., T. Shimamoto, L. Yao, T. Togo, and H. Kitajima (2014), A rotary-shear low to high-velocity friction apparatus in Beijing to study rock friction at plate to seismic slip rates, *Earthquake Sci.*, *27*(5), 469–497.

Marone, C., C. B. Raleigh, and C. H. Scholz (1990), Frictional behavior and constitutive modeling of simulated fault gouge, *J. Geophys. Res.*, *95*, 7007–7025, doi:10.1029/JB095iB05p07007.

Mizoguchi, K., M. Takahashi, K. Masuda, and E. Fukuyama (2007a), Fault strength drop due to phase transitions in the pore fluid, *Geophys. Res. Lett.*, *34*, L09313, doi:10.1029/2007GL029345.

Mizoguchi, K., T. Hirose, T. Shimamoto, and E. Fukuyama (2007b), Reconstruction of seismic faulting by high-velocity friction experiments: An example of the 1995 Kobe earthquake, *Geophys. Res. Lett.*, *34*, L01308, doi:10.1029/2006GL027931.

Niemeijer, A., G. Di Toro, S. A. F. Smith, A. W. Griffith, A. Bistacchi, and S. Nielsen (2012), Inferring earthquake physics and chemistry using an integrated field and laboratory approach, *J. Struct. Geol.*, *39*, 2–36.

Noda, H., and L. Lapusta (2013), Stable creeping fault segments can become destructive as a result of dynamic weakening, *Nature*, *518*, doi:10.1038/nature11703.

Peterson, E., and J. A. Mavrogenes (2014), Linking high-grade gold mineralization to earthquake-induced fault-valve processes in the Porgera gold deposit, Papua New Guinea, *Geology*, *42*, 383–386.

Platt, J. D., B. Proctor, T. M. Mitchell, G. Hirth, D. L. Goldsby, G. Di Toro, N. M. Beeler, and T. E. Tullis (2014), The role of gouge and temperature on flash heating and its hysteresis, Abstract S11C-4360 presented at 2014 Fall Meeting, AGU, San Francisco, Calif.

Rempe, M., S. A. F. Smith, F. Ferri, T. M. Mitchell, and G. Di Toro (2014), Clast-cortex aggregates in experimental and natural calcite-bearing fault zones, *J. Struct. Geol.*, *68*, 142–157.

Rice, J. R. (2006), Heating and weakening of faults during earthquake slip, *J. Geophys. Res.*, *111*, B05311, doi:10.1029/2005JB004006.

Sibson, R. H., F. Robert, and K. H. Poulsen (1988), High-angle reverse faults, fluid-pressure cycling, and mesothermal gold–quartz deposits, *Geology*, *16*, 551–555.

Smith, S. A. F., G. Di Toro, S. Kim, J. H. Ree, S. Nielsen, A. Billi, and R. Spiess (2013), Co-seismic recrystallization during shallow earthquake slip, *Geology*, *41*, 63–66.

Smith, S. A. F., S. Nielsen, and G. Di Toro (2015), Strain localization and the onset of dynamic weakening in calcite fault gouge, *Earth Planet. Sci. Lett.*, *413*, 25–36.

Sulem, J., P. Lazar, and I. Vardoulakis (2007), Thermo-poro-mechanical properties of clayey gouge and application to rapid fault shearing, *Int. J. Numer. Anal. Meth. Geomech.*, *31*, 523–540.

Tanaka, H., W. M. Chen, C. Y. Wang, K. F. Ma, N. Urata, J. Mori, and M. Ando (2006), Frictional heat from faulting of the 1999 Chi-Chi, Taiwan earthquake, *Geophys. Res. Lett.*, *33*, L16316, doi:10.1029/2006GL026673.

Tanikawa, W., and T. Shimamoto (2009), Frictional and transport properties of the Chelungpu fault from shallow borehole data and their correlation with seismic behavior during the 1999 Chi-Chi earthquake, *J. Geophys. Res.*, *114*, B01402, doi:10.1029/2008JB005750.

Tanikawa, W., O. Tadai, and H. Mukoyoshi (2015), Permeability changes in simulated granite faults during and after frictional sliding, *Geofluids*, *14*, 481–494.

Togo, T., T. Shimamoto, S. Ma, and T. Hirose (2011), High-velocity frictional behavior of Longmenshan fault gouge from Hongkou outcrop and its implications for dynamic weakening of fault during the 2008 Wenchuan earthquake, *Earthquake Sci.*, *24*, 267–281.

Togo, T., T. Shimamoto, J.-J. Dong, C.-T. Lee, and C.-M. Yang (2014), Triggering and runaway processes of catastrophic Tsaoling landslide induced by the 1999 Taiwan Chi-Chi earthquake, as revealed by high-velocity friction experiments, *Geophys. Res. Lett.*, *41*, 1907–15, doi:10.1002/2013GL059169.

Ujiie, K., A. Tsutsumi, and J. Kameda (2011), Reproduction of thermal pressurization and fluidization of clay-rich fault gouges by high-velocity friction experiments and implications for seismic slip in natural faults Rick Sibson, *Geol. Soc. (Lond.) Spec. Publ.*, *359*, 267–285.

Ujiie, K., et al. (2013), Low coseismic shear stress on the Tohoku-oki megathrust determined from laboratory experiments, *Science*, *342*, 1211–1214.

Violay, M., S. Nielsen, B. Gibert, B. Gibert, E. Spagnuolo, A. Cavallo, P. Azais, S. Vinciguerra, and G. Di Toro (2013), Effect of water on the frictional behavior of cohesive rocks during earthquakes, *Geology*, doi:10.1130/G34916.1.

Violay, M., G. Di Toro, S. Nielsen, E. Spagnuolo, and J. P. Burg (2015), Thermo-mechanical pressurization of experimental faults in cohesive rocks during seismic slip, *Earth Planet. Sci. Lett.*, *429*, 1–10.

Weatherley, D. K., and R. W. Henley (2013), Flash vaporization during earthquakes evidence by gold deposits, *Nat. Geosci.*, *6*, 294–298.

Wibberley, C. A. J., and T. Shimamoto (2005), Earthquake slip weakening and asperities explained by thermal pressurization, *Nature*, *436*, 689–692.

Xu, X., X. Wen, G. Yu, G. Chen, Y. Klinger, J. Hubbard, and J. Shaw (2009), Coseismic reverse- and oblique-slip surface faulting generated by the 2008 M_w 7.9 Wenchuan earthquake, China, *Geology*, *37*(6), 515–518.

Yao, L., S. Ma, A. R. Niemeijer, T. Shimamoto, and J. D. Platt (2016), Is frictional heating needed to cause dramatic weakening of nanoparticle gouge during seismic slip? Insights from friction experiments with variable thermal evolutions, *Geophys. Res. Lett.*, *43*, 6852–6860, doi:10.1002/2016GL069053.